The role of force field parameter uncertainty in the prediction of the pressure-viscosity coefficient

Richard A. Messerly

Thermodynamics Research Center, National Institute of Standards and Technology, Boulder, Colorado, 80305

Michelle C. Anderson

Thermodynamics Research Center, National Institute of Standards and Technology, Boulder, Colorado, 80305

S. Mostafa Razavi

Department of Chemical and Biomolecular Engineering, The University of Akron, Akron, Ohio, 44325-3906

J. Richard Elliott

Department of Chemical and Biomolecular Engineering, The University of Akron, Akron, Ohio, 44325-3906

Abstract

In response to the 10th Industrial Fluid Properties Simulation Challenge, we report viscosity (η) estimates of 2,2,4-trimethylhexane at 293 K for a range of pressures (P) from 0.1 MPa to 1000 MPa. The Potoff force field is utilized in this study, as a previous study demonstrated that it provides reliable estimates of η with respect to P. Whereas most studies report only the uncertainties associated with random fluctations in the simulation output, we investigate the effect of the uncertainties arising from the force field non-bonded and torsional parameters. Although the uncertainties increase substantially with increasing pressure, we obtain quantitative evidence that supports so-called super-Arrhenius behavior with an inflection point in an $\ln(\eta)$-P plot around 500 MPa. The pressure-viscosity coefficient as a function of pressure is reported for several different empirical fitting models.

Keywords:

Email addresses: `richard.messerly@nist.gov` (Richard A. Messerly), `michelle.anderson@nist.gov` (Michelle C. Anderson), `sr87@zips.uakron.edu` (S. Mostafa Razavi), `elliot1@uakron.edu` (J. Richard Elliott)

Uncertainty Quantification, Bayesian Inference, Thermophysical Properties, Shear Viscosity, Molecular Dynamics Simulation

1. Introduction

The Industrial Fluid Properties Simulation Challenge (IFPSC) is an open international competition aimed at aligning the molecular simulation community, which is primarily academic, with the goals of industrial research. The present work is a submission to the 10th Industrial Fluid Properties Simulation Challenge (IFPSC10). The 10th challenge is to predict the viscosity (η) of 2,2,4-trimethylhexane (224TMH) over a wide range of pressures (P), namely, from 0.1 MPa (atmospheric) to 1000 MPa, at a constant temperature (T) of 293 K.

The practical application of IFPSC10 is elastohydrodynamic lubrication (EHL), where knowledge of the pressure-viscosity relationship is paramount. The challenge compound was chosen as an ideal lubricating oil candidate for which no published experimental viscosity data are available above ambient pressure. Experimental measurements are performed by Scott Bair of Georgia Tech with a sample of greater than 98% purity. The estimated experimental uncertainties for η, T, and P are, respectively, 3%, 0.3 K, and the greater of 1 MPa and 0.4 %.

Classical film thickness formulas rely heavily on the so-called pressure-viscosity coefficient (α), which is essentially an Arrhenius-like activation parameter that is obtained from the slope for an $\ln(\eta)$-P plot. However, faster-than-exponential, a.k.a. super-Arrhenius, dependence on pressure has been observed through experimental viscometry measurements for nearly a century. This super-Arrhenius trend is typically manifest by an inflection point in the $\ln(\eta)$-P plot. While this behavior is common in experimental measurements, we are not aware of any rheological molecular simulation studies that have addressed this topic, as most simply assume an Arrhenius relationship when reporting α [**?** 1, 2]. IFPSC10 is an ideal opportunity to demonstrate whether or not molecular simulation can provide evidence supporting or opposing the existence of super-Arrhenius

behavior.

In a previous study, we investigated the adequacy of four different force fields for predicting the viscosity-pressure trend, namely, the Transferable Potentials for Phase Equilibria (TraPPE-UA [3, 4, 5]), Transferable Anisotropic Mie (TAMie) [6, 7], Potoff [8, 9], and fourth generation anisotropic-united-atom (AUA4) [10, 11]. Each force field uses a united-atom (UA) Mie λ-6 (generalized Lennard-Jones, LJ) functional form. The comparisons with experimental data were made for saturated liquid viscosity ($\eta_{\text{liq}}^{\text{sat}}$) and compressed liquid viscosity ($\eta_{\text{liq}}^{\text{comp}}$) at 293 K from atmospheric pressure to 1000 MPa. The compounds in question were n-alkanes ranging in carbon number from ethane to n-docosane and branched alkanes ranging in size from 2-methylpropane to 2,2,4-trimethylpentane (224TMP). The 224TMP results at high pressures are especially useful as this compound is a close analogue to the challenge compound and, in contrast with 224TMH, 224TMP has been well studied experimentally.

While TraPPE and AUA4 (LJ 12-6 based potentials) under predict $\eta_{\text{liq}}^{\text{sat}}$ by greater than 30 % for all compounds studied, TAMie (Mie 14-6) and Potoff (Mie 16-6) predict $\eta_{\text{liq}}^{\text{sat}}$ within 10 % for most compounds. For $\eta_{\text{liq}}^{\text{comp}}$, TAMie is the most reliable at predicting the viscosity-density dependence, while Potoff significantly over estimates $\eta_{\text{liq}}^{\text{comp}}$ with respect to density. However, since Potoff also over estimates pressure at high densities [12], the viscosity-pressure trend for Potoff is remarkably accurate even at pressures approaching 1000 MPa. In particular, the Potoff force field predicts the viscosity-pressure trend for 2,2,4-trimethylpentane to within 10 % accuracy. For this reason, we chose to implement the Potoff Mie 16-6 force field for the challenge of predicting η and α of the challenge compound. We should note, however, that our previous study did not provide any definitive evidence that the Potoff force field could predict a super-Arrhenius trend for the compounds studied.

One of the entry guidelines for IFPSC is "an analysis of the uncertainty in the calculated results." Traditionally, simulation uncertainties are limited to the random fluctuations of simulation output and/or the uncertainty related to data post-processing. This

class of uncertainty is referred to as "numerical uncertainty" (frequently referred to as "statistical uncertainty"). Two other classes of uncertainty, namely, "parameter uncertainty" and "functional form uncertainty" (also referred to as "model uncertainty") are typically ignored in uncertainty quantification (UQ) due to the increased computational cost. The latter refers to the uncertainty associated with the choice of force field functional form, while the former refers to the uncertainty in the force field parameters for a given force field functional form.

Quantifying the functional form uncertainty is an extremely difficult task, as it often requires performing simulations with numerous force field functional forms. For this reason, we focus on numerical and parameter uncertainties without addressing functional form uncertainties. Specifically, we apply bootstrap re-sampling and Bayesian inference Markov Chain Monte Carlo (MCMC) to quantify numerical and parameter uncertainties, respectively. The chosen functional form is the same as the Potoff force field, namely, a united-atom, fixed bond length, harmonic angular potential, cosine series torsional potential, and a Mie 16-6 non-bonded potential (see Section 2.1 for details). As viscosity is highly sensitive to the non-bonded [13, 14] and torsional [15, 16] potentials, we limit our parameter uncertainty investigation to the non-bonded and torsional parameters.

The outline for the present work is the following. Section 2 explains the force field, simulation methodology, and data analysis. Section 3 presents the simulation results, with an emphasis on uncertainty quantification. Section 4 discusses some important observations and limitations. Section 5 recaps the primary conclusions from this work.

2. Methods

2.1. Force fields

We utilize the Potoff force field as it provides reliable estimates of the η-P dependence for normal and branched alkanes that are similar to the challenge compound [14]. In addition, we quantify the uncertainty in η that arises from uncertainties in the non-bonded Mie 16-6 and torsional parameters. The parameter uncertainties are obtained using Bayesian

inference Markov Chain Monte Carlo (MCMC). This analysis is performed sequentially. First, we include only the non-bonded uncertainties (referred to as MCMC-nb). Then, we include both the non-bonded and torsional uncertainties (MCMC-nb-tors). This sequential approach provides insight into which source of uncertainty has a greater impact on η.

The Potoff Mie λ-6 force field utilizes united-atom (UA) sites, where 2,2,4-trimethylhexane is represented with CH_3, CH_2, CH, and C UA sites. Neighboring UA sites are separated by a fixed 0.154 nm bond length. Note that we observed in our previous study that the use of flexible bonds can impact η by several percent. Therefore, the choice of fixed bonds was not arbitrary and is a possible source of uncertainty for which we did not rigorously account.

The angular contribution to energy is computed using a harmonic potential:

$$u^{\text{bend}} = \frac{k_\theta}{2} \left(\theta - \theta_0\right)^2 \tag{1}$$

where u^{bend} is the bending energy, θ is the instantaneous bond angle, θ_0 is the equilibrium bond angle (see Table 1), and k_θ is the harmonic force constant with $k_\theta/k_B = 62500\,\text{K/rad}^2$ for all bonding angles, where k_B is the Boltzmann constant.

Table 1: Equilibrium bond angles (θ_0) [4, 9]. CH_i and CH_j represent CH_3, CH_2, CH, or C sites.

Bending sites	θ_0 (degrees)
CH_i-CH_2-CH_j	114.0
CH_i-CH-CH_j	112.0
CH_i-C-CH_j	109.5

Dihedral torsional interactions are determined using a modified cosine series:

$$
\begin{aligned}
u^{\text{tors}} &= c_0 + c_1[1 + \cos\phi] + c_2[1 - \cos 2\phi] + c_3[1 + \cos 3\phi] + A_s \sin^2\left(\frac{3\phi}{2} + 180°\right) \\
&= (c_0 - A_s) + c_1[1 + \cos\phi] + c_2[1 - \cos 2\phi] + \left(c_3 + \frac{A_s}{2}\right)[1 + \cos 3\phi] \quad (2)
\end{aligned}
$$

5

where u^{tors} is the torsional energy, ϕ is the dihedral angle, c_n are the Fourier constants used in the Potoff force field and listed in Table 2, and $A_{\text{s}} \sin^2\left(\frac{3\phi}{2} + 180°\right)$ is an additional term proposed by 15 to shift the torsional barrier heights. Note that ϕ is defined using a convention similar to IUPAC where $\phi = 180°$ for the *trans* conformation, whereas 15 defines the *trans* conformation as $0°$ or $360°$ deg, hence the $+180°$ term. As $\sin^2\left(\frac{3\phi}{2} + 180°\right)$ has a maximum value of 1 at $0°$, $120°$, $240°$, and $360°$, u^{tors} is shifted by A_{s} at these dihedral angles. By contrast, this additional term does not shift u^{tors} for dihedral angles of $0°$, $180°$, and $300°$, which correspond to the equilibrium conformations of *gauche⁻*, *trans*, and *gauche⁺*, respectively. Clearly, the non-shifted Potoff torsional potential is obtained only when $A_{\text{s}} = 0$.

Table 2: Fourier constants (c_n/k_{B}) and shifting parameter $(A_{\text{s}}/k_{\text{B}})$ in units of K for Potoff force field [4, 9]. CH_i and CH_j represent CH_3, CH_2, CH, or C sites.

Torsion sites	c_0/k_{B}	c_1/k_{B}	c_2/k_{B}	c_3/k_{B}	$A_{\text{s}}/k_{\text{B}}$
CH_i-CH_2-CH-CH_j	-251.06	428.73	-111.85	441.27	0.0
CH_i-CH_2-C-CH_j	0.0	0.0	0.0	461.29	0.0

15 set A_{s} equal to 40% and 15% of the maximum dihedral barrier for the CH_3-CH_2-CH_2-CH_2 and CH_2-CH_2-CH_2-CH_2 torsional potentials, respectively. This corresponds to $A_{\text{s}}/k_{\text{B}} \approx 1000$ K and ≈ 375 K for the CH_3-CH_2-CH_2-CH_2 and CH_2-CH_2-CH_2-CH_2 torsional potentials, respectively. The primary reason why 15 introduced this additional term was to increase the torsional barriers and, thereby, increase the viscosity obtained with the AUA4m force field. This methodology works fairly well for Lennard-Jones 12-6 force fields, which systematically under predict viscosity by greater than 30 %. However, since the Potoff Mie 16-6 potential is already quite reliable for predicting viscosity, we would expect significant over prediction of viscosity if we coupled the Potoff Mie 16-6 potential with $A_{\text{s}}/k_{\text{B}} \gg 0$ K.

The actual reason we include the additional term, however, is to provide a simple

method for quantifying the uncertainty in the torsional potential. Specifically, we assume that A_s follows a normal distribution with a mean value of zero and a standard deviation equal to $0.075 \times \max(u^{\text{tors}}_{\text{Potoff}})\ 0.075 \times \max(u^{\text{tors}}_{A_s=0})$. The standard deviation is assigned such that the 95% confidence interval is equal to 15% the maximum barrier height for the Potoff torsional potential. We use a normal distribution such that the uncertainty in the dihedral barriers is symmetric, i.e., unlike 15 we do not assume that the dihedral barriers must be increased unilaterally. Figure 1 compares the Potoff and MCMC torsional potentials. The insets also depict the normal distribution and the randomly sampled MCMC A_s sets. Note that the challenge compound consists of four $CH_i-CH_2-CH-CH_j$ torsions and three $CH_i-CH_2-C-CH_j$ torsions.
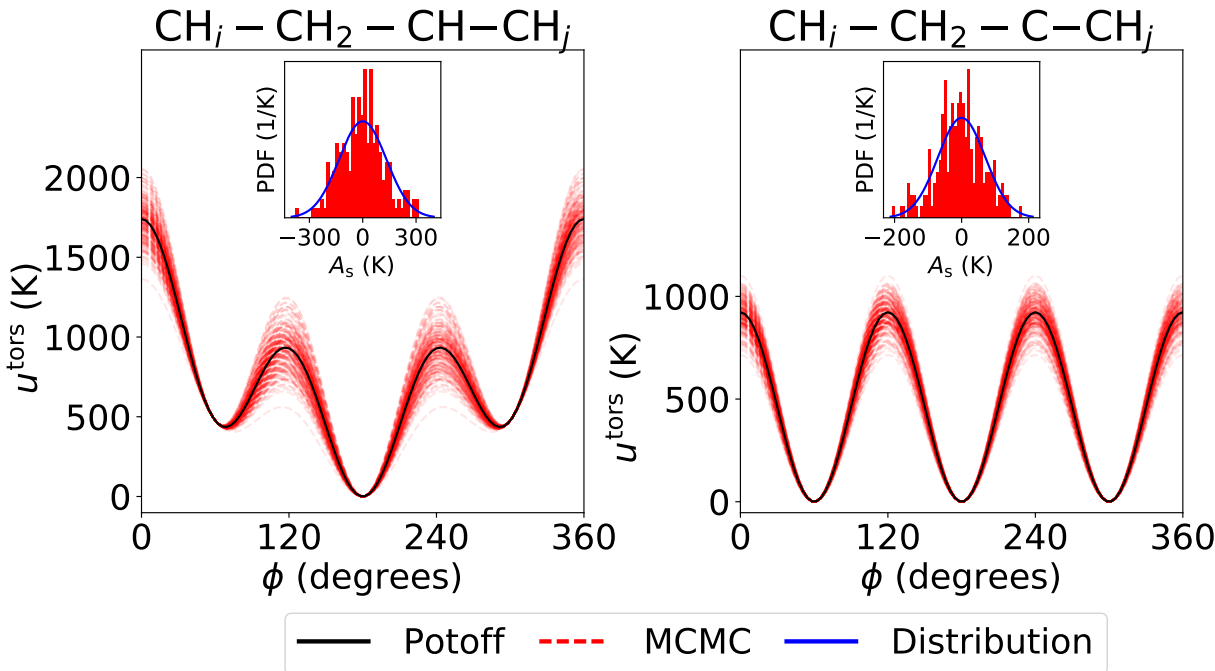

Figure 1: Uncertainty in dihedral potentials. Black line is the Potoff torsional potential. Red lines are the 200 MCMC sampled parameter sets used in this study. Insets show the distribution for A_s. Both u^{tors} and A_s are expressed in units of K, i.e., divided by k_{B}.

Non-bonded interactions between sites located in two different molecules or separated by more than three bonds within the same molecule are calculated using a Mie λ-6

potential (of which the Lennard-Jones, LJ, 12-6 is a subclass) [17]:

$$u^{\text{vdw}}(\epsilon, \sigma, \lambda; r) = \left(\frac{\lambda}{\lambda - 6}\right) \left(\frac{\lambda}{6}\right)^{\frac{6}{\lambda - 6}} \epsilon \left[\left(\frac{\sigma}{r}\right)^{\lambda} - \left(\frac{\sigma}{r}\right)^{6}\right] \tag{3}$$

where u^{vdw} is the van der Waals interaction, σ is the distance (r) where $u^{\text{vdw}} = 0$, $-\epsilon$ is the energy of the potential at the minimum $\left(\text{i.e., } u^{\text{vdw}} = -\epsilon \text{ and } \frac{\partial u^{\text{vdw}}}{\partial r} = 0 \text{ for } r = r_{\text{min}}\right)$, and λ is the repulsive exponent.

The non-bonded Potoff Mie λ-6 force field parameters are provided in Table 3. Note that Potoff reports a "generalized" and "short/long" (S/L) CH and C parameter set. The "generalized" CH and C parameter set is an attempt at a completely transferable set, while the "short" and "long" parameters are implemented when the number of carbons in the backbone is ≤ 4 and > 4, respectively. The Potoff results presented in this study are obtained with the "long" parameters. (Note the discrepancy between the generalized C parameters reported in Table 1 of Reference 9 and the optimal region depicted in Figure 1 of Reference 9.)

Table 3: Non-bonded Potoff Mie λ-6 parameters. The "short/long" Potoff CH and C parameters are included in parentheses.

	Potoff (S/L)		
United-atom	ϵ/k_{B} (K)	σ (nm)	λ
CH_3	121.25	0.3783	16
CH_2	61	0.399	16
CH	15 (15/14)	0.46 (0.47/0.47)	16
C	1.05 (1.45/1.2)	0.605 (0.61/0.62)	16

Non-bonded parameters between two different site types (i.e., cross-interactions) are determined using Lorentz-Berthelot combining rules [18] for ϵ and σ and an arithmetic mean for the repulsive exponent λ (as recommended in Reference 8):

$$\epsilon_{ij} = \sqrt{\epsilon_{ii}\epsilon_{jj}} \tag{4}$$

8

$$\sigma_{ij} = \frac{\sigma_{ii} + \sigma_{jj}}{2} \tag{5}$$

$$\lambda_{ij} = \frac{\lambda_{ii} + \lambda_{jj}}{2} \tag{6}$$

where the ij subscript refers to cross-interactions and the subscripts ii and jj refer to same-site interactions.

The MCMC non-bonded parameters for CH_3 and CH_2 ($\epsilon_{CH_3}, \sigma_{CH_3}, \epsilon_C H_2$, and $\sigma_C H_2$) were reported previously [12]. These parameters were obtained using a likelihood function based on saturated liquid density and saturated vapor pressure data for ethane, propane, n-butane, and n-octane. By contrast, the MCMC parameters for CH and C ($\epsilon_{CH}, \sigma_{CH}, \epsilon_C$, and σ_C) were obtained from the scoring function reported in Reference 9 that depends on several vapor-liquid coexistence properties for a wide range of branched alkanes. Translating the scoring function into a Bayesian context is achieved by modeling the ϵ-σ CH and C uncertainties with a multivariate normal distribution, where the covariance matrix was obtained by assuming that the "generalized" CH and C parameter set should not be distinguishable (at the 95 % confidence level) from the "long" parameter set.

Note that this approach applies the common assumption of transferability between UA sites. In addition, the parameter correlation between different UA sites, e.g., between σ_{CH_3} and $\sigma_C H$, are assumed to be negligible. In other words, we only account for the parameter correlation between ϵ-σ sets of the same UA site. The reason for this assumption is the reduced complexity of performing four independent two-dimensional MCMC runs compared to one eight-dimensional MCMC run.

Note that the uncertainties in the CH and C non-bonded parameters are considerably larger than those for CH_3 and CH_2. The CH_3 parameters contribute to the majority of non-bonded interactions (both between different molecules as well as within the same molecule). Therefore, the relatively small uncertainties assigned to the CH_3 parameters are likely the cause for the negligible impact of non-bonded uncertainties.

Two important assumptions are made in this UQ analysis. First, we not only apply the common assumption of transferability between UA sites, but we also assume that there is
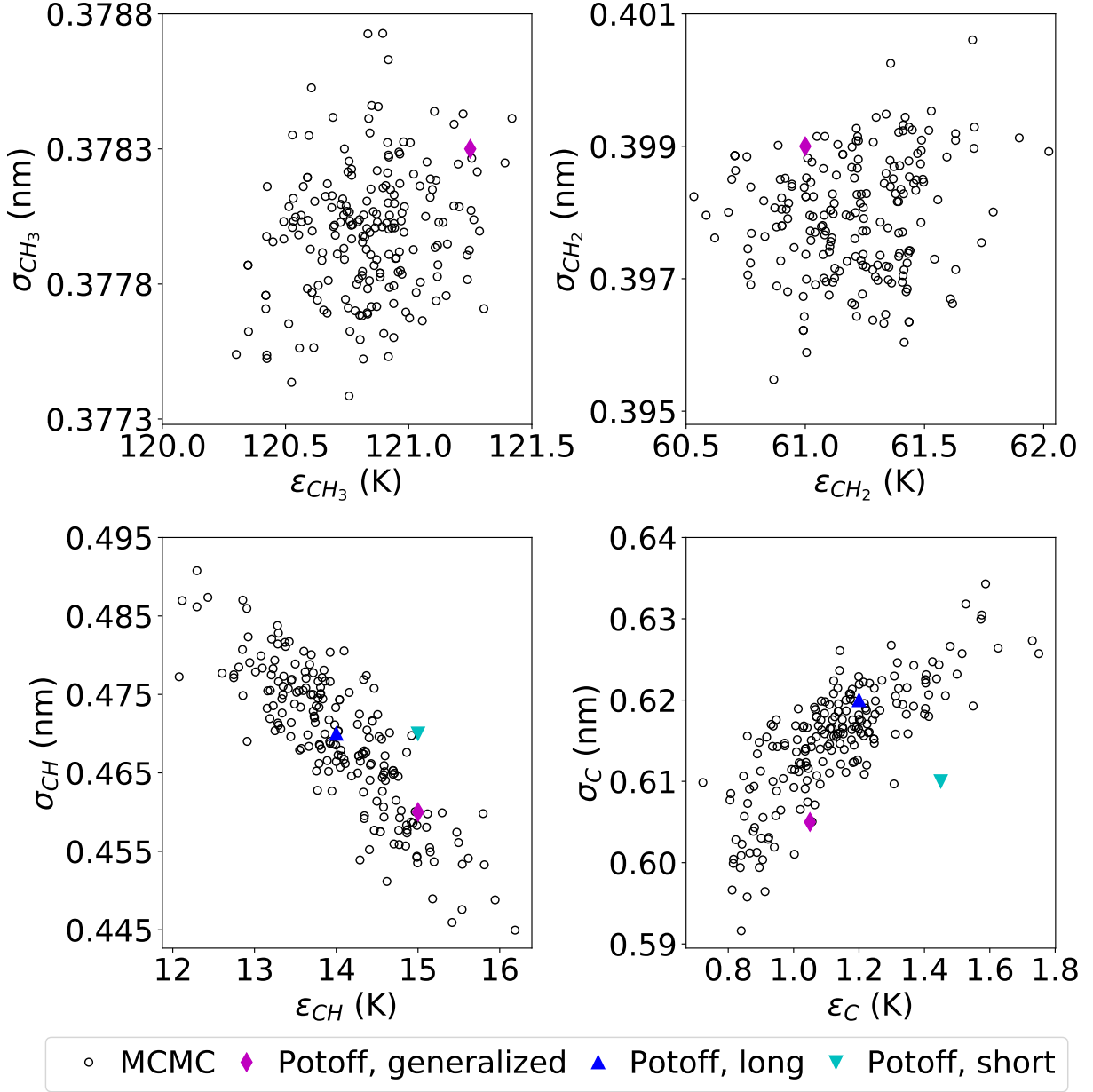
Figure 2: Uncertainty in non-bonded parameters determined with Markov Chain Monte Carlo (MCMC). The Potoff generalized and S/L parameters are also included as a reference. [8, 9]

zero correlation between different UA sites [19]. Second, we assume that the uncertainties obtained from as the likelihood and scoring functions depend only on thermodynamic properties at vapor-liquid coexistence conditions, we assume that the In other words, a variation be The CH_3 parameters for ethane are assumed to be transferable to longer *n-*

alkanes

In summary, the following assumptions are made in this uncertainty analysis:

1. Correlation between different UA sites is zero, i.e., all UA sites are transferable

2. $\lambda = 16$, i.e., only ϵ and σ have non-zero uncertainty

3. Likelihood function and scoring function depend only on thermodynamic properties at vapor-liquid coexistence conditions

1. Potoff force field proved to be most reliable in previous study

2. United-atom, Mie 16-6

3. AUA4m considered modifying torsional barriers for CH_2-CH_2 by 15 % and 40 % for internal and terminal torsions, respectively.

4. Include uncertainty in ϵ, σ, and U^{tors}

5. Plots of MCMC samples and maybe the Mie potentials and torsional barriers explicitly

2.2. Simulation set-up

Historically, non-equilibrium molecular dynamics (NEMD) has been preferred for highly viscous systems [1, 2]. However, in our recent publication we successfully predicted the viscosity of 2,2,4-trimethylpentane at 293 K and 1000 MPa (the highest pressure required for the challenge) with equilibrium molecular dynamics (EMD). Consistent with our previous study, we use EMD for all pressures in the challenge.

Equilibrium molecular dynamics simulations are performed using GROMACS version 2018 with "mixed" (single and double) precision [20]. GROMACS is compiled using GNU 7.3.0, OpenMPI enabled, and GPU support disabled. The simulations are run using Linux 4.4.0-112-generic x86_64 on an Intel(R) Xeon(R) CPU E5-2699 v4 @ 2.20GHz machine. Example GROMACS input files (.top, .gro. and .mdp) with corresponding shell and python scripts for preparing, running, and analyzing simulations are provided as Supporting Information.

We utilize the same simulation specifications as our previous study BLANK. The general simulation specifications are provided in Table 4. Our previous study demonstrates that, for compounds smaller than n-dodecane, the correct system dynamics are obtained using a 2 fs time-step and 1.4 nm non-bonded cut-off distance with analytical tail corrections [21]. Our previous study also shows that finite size effects are negligible for a 400 molecule system.

Table 4: General simulation specifications.

Time-step (fs)	2
Cut-off length (nm)	1.4
Tail-corrections	U and P
Constrained bonds	LINCS [22, 23]
LINCS-order	8
Number of molecules	400

We perform a sequence of six simulation stages: energy minimization, NPT equilibration, NPT production, energy minimization, NVT equilibration, and NVT production. Table 5 lists the integrators, thermostats, barostats, and simulation time used for each NPT and NVT equilibration and production stage. These specifications are also the same as our previous study, with the exception of the NVT production simulation times, which are state point dependent. The specific production times for the NVT production stage are provided in Table 6.

A large number of replicate simulations are required at each state point to improve the precision and to provide more rigorous estimates of uncertainty [24, 25]. We utilize between 30 and 80 independent replicates when simulating the Potoff force field, while we use 200 replicates for the MCMC parameter sets. To ensure independence between replicates, the entire series of simulation stages are repeated for each replicate where the initial energy minimization stage starts with a different pseudo-random configuration

Table 5: Simulation specifications for equilibration (Equil.) and production (Prod.) stages.

	NPT Equil.	NPT Prod.	NVT Equil.	NVT Prod.
Simulation time (ns)	1	1	1	1 to 32
Integrator	Velocity Verlet	Leap frog	Velocity Verlet	Velocity Verlet
Thermostat	Velocity rescale	Nosé-Hoover	Nosé-Hoover	Nosé-Hoover
Thermostat time-constant (ps)	1.0	1.0	1.0	1.0
Barostat	Berendsen	Parrinello-Rahman	N/A	N/A
Barostat time-constant (ps)	1.0	5.0	N/A	N/A
Barostat compressibility (1/bar)	4.5E-5	4.5E-5	N/A	N/A

Table 6: State point specific production times. Pressure is prescribed only in NPT equilibration and production stages.

Pressure (MPa)	NVT Prod. time (ns)
0.1	1
25	1
50	1
100	1
150	1
250	2
400	4
500	8
600	8
700	16
800	16
900	24
1000	32

and the initial velocities are randomized for each equilibration stage.

2.3. Data analysis

The analysis for the Potoff Mie λ-6 force field simulation results is identical to that prescribed in our previous study (see Reference BLANK). In brief, we implement the Green-Kubo "time-decomposition" analysis [24, 25]

$$\eta(t) = \frac{V}{k_{\mathrm{B}}TN_{\mathrm{reps}}} \sum_{n=1}^{N_{\mathrm{reps}}} \int_0^t dt' \left\langle \tau_{\alpha\beta,n}(t')\tau_{\alpha\beta,n}(0) \right\rangle_{t_0,\alpha\beta} \tag{7}$$

where t is time, V is volume, N_{reps} is the number of independent replicate simulations, α and β are $x, y,$ or z Cartesian coordinates, $\tau_{\alpha\beta,n}$ is the α-β off-diagonal stress tensor

element for the nth replicate, and $\langle \cdots \rangle_{t_0, \alpha\beta}$ denotes an average over time origins (t_0) and $\tau_{\alpha\beta}$.

$\tau_{\alpha\beta, n}$ is recorded every 6 fs (3 time-steps), Equation 7 averages the independent replicate simulations, twelve different time-origins, and all three unique off-diagonal stress tensor components.

The "true" viscosity, i.e., the infinite-time-limit viscosity, is obtained by evaluating Equation 7 as $t \to \infty$. As the long-time tail does not converge, we fit the "running integral" to a double-exponential function

$$\eta(t) = A\alpha\tau_1 \left(1 - \exp\left(-t/\tau_1\right)\right) + A(1 - \alpha)\tau_2 \left(1 - \exp\left(-t/\tau_2\right)\right) \tag{8}$$

where A, α, τ_1, and τ_2 are fitting parameters and $\eta^\infty = A\alpha\tau_1 + A(1-\alpha)\tau_2$ is the infinite-time-limit viscosity. We fit Equation 8 using a weighted sum-squared-error objective function where the weights are equal to the inverse of the squared standard deviation (σ_η^2). The standard deviation with respect to time of the replicate simulations is fit to the model At^b, where A and b are fitting parameters. To improve the fit of Equation 8, we employ both a long-time and short-time cut-off. Specifically, only data for $t > 3$ ps are included in the fit, while data where $\eta(t) > 0.4 \times \eta^\infty$ are excluded [24, 25].

The uncertainty in η^∞ is obtained by bootstrap re-sampling. Specifically, the fitting process described previously is repeated hundreds of times using randomly selected subsets of replicate simulations. For the Potoff results, each replicate simulation utilizes the same force field parameters. By contrast, the MCMC-nb and MCMC-nb-tors replicates utilize different parameter sets. The 95 % confidence interval is obtained from the distribution of bootstrap estimates for η^∞. An example of the MCMC process is provided in Section SI.II of Supporting Information.

The simulation results are fit to four different empirical models from which the pressure-viscosity coefficient (α) is calculated. As viscosity ranges over several orders of magnitude, the objective function for fitting is the sum-squared-error of $\log_{10}(\eta)$. Only the MCMC-nb-tors values are included in the fit, as these simulation results account for more sources of uncertainty than the Potoff and MCMC-nb results. The pressure-viscosity co-

efficient for each empirical fit is obtained by differentiating $ln(\eta)$ with respect to P.

The first empirical model we implement is the traditional Barus expression [26]

$$\eta = \eta_0 \exp(\alpha P) \tag{9}$$

where η_0 and α are fitting parameters. The second model is the popular Roelands equation [27]

$$\eta = \eta_p \left(\frac{\eta_0}{\eta_p}\right)^{\left(\frac{P_p - P}{P_p}\right)^Z} \tag{10}$$

where η_0 and Z are fitting parameters and $\eta_p = 6.31 \times 10^{-5}$ Pa-s and $P_p = -0.196$ GPa. The third model is an alternative form of Equation 10 where eta_p and P_p are additional fitting parameters (rather than fixed constants). This four parameter Roelands equation, which we refer to as "Roelands-Modified," is more flexible than the standard Roelands model and can predict super-Arrhenius behavior. The fourth model is a hybrid McEwen-Paluch expression [28]

$$\eta = \eta_0 \left(1 + \frac{a_0}{q}P\right)^q \exp\left(\frac{C_F P}{P_\infty - P}\right) \tag{11}$$

where η_0, a_0, q, C_F, and P_∞ are fitting parameters. Note that, although the Roelands-Modified equation can predict super-Arrhenius behavior, only the McEwen-Paluch model is capable of representing an inflection point, i.e., a transition from Arrhenius to super-Arrhenius behavior. By contrast, the Barus and Roelands models are only capable of fitting sub-Arrhenius and Arrhenius-like data.

3. Results

Tabulated values for viscosity, density, and pressure at the prescribed state points are provided in Table 7. These values are also depicted in Figure 3 along with the available experimental data point and model fits to simulation data.

Figure 4 compares the different sources of uncertainty. The Potoff results only account for numerical uncertainties while MCMC-nb also accounts for non-bonded parameter uncertainty and MCMC-nb-tors also accounts for torsional uncertainties. Note that the

Table 7: Simulation results for Potoff, MCMC-Mie, and MCMC-Mie-tors.

		Potoff		MCMC-Mie		MCMC-Mie-tors	
T (K)	P (MPa)	ρ (kg/m^3)	η (Pa-s)	ρ (kg/m^3)	η (Pa-s)	ρ (kg/m^3)	η (Pa-s)

reason why the MCMC-nb and MCMC-nb-tors uncertainties are larger than the Potoff uncertainties is because the latter uses fewer replicate simulations. When the non-bonded and torsional uncertainties are negligible compared to the numerical uncertainties, this increase in N_{reps} reduces the numerical uncertainty and, consequently, the overall uncertainty decreases as well.

The predicted pressure-viscosity coefficient (α), as determined by fitting the MCMC-nb-tors results to Equations 9, 10, and 11, are presented in Figure 5. The uncertainties in α are obtained with bootstrap re-sampling, where a single η value is randomly selected from the MCMC-nb-tors distribution. The traditional Barus α value is constant with respect to pressure. The Roelands α value actually decreases with increasing pressure, while the Roelands, Modified α value does increase but without a change in slope. Only the McEwen-Paluch α value shows the marked change in slope which corresponds to an inflection point in the $\ln(\eta)$-P plot. The α magnitude are all reasonable (i.e., similar in magnitude to other lubricants) over the entire range of pressures.

Although the hybrid McEwen-Paluch model clearly reproduces the simulation results with lower deviations than those of the Roelands and Barus models, this should be anticipated considering the McEwen-Paluch model has five fitting parameters while the Barus and Roelands models only have two. Note that the four parameter Roelands-Modified model also has lower deviations than the Roelands and Barus models. Therefore, it is possible that the McEwen-Paluch model is actually over-fit to our simulation results. To assess this possibility, Figure 6 presents the cross-validation results for each model. Specifically, we implement a Monte Carlo cross-validation scheme where thousands of random sub-samples are selected for the training and testing set. Approximately 70 % of
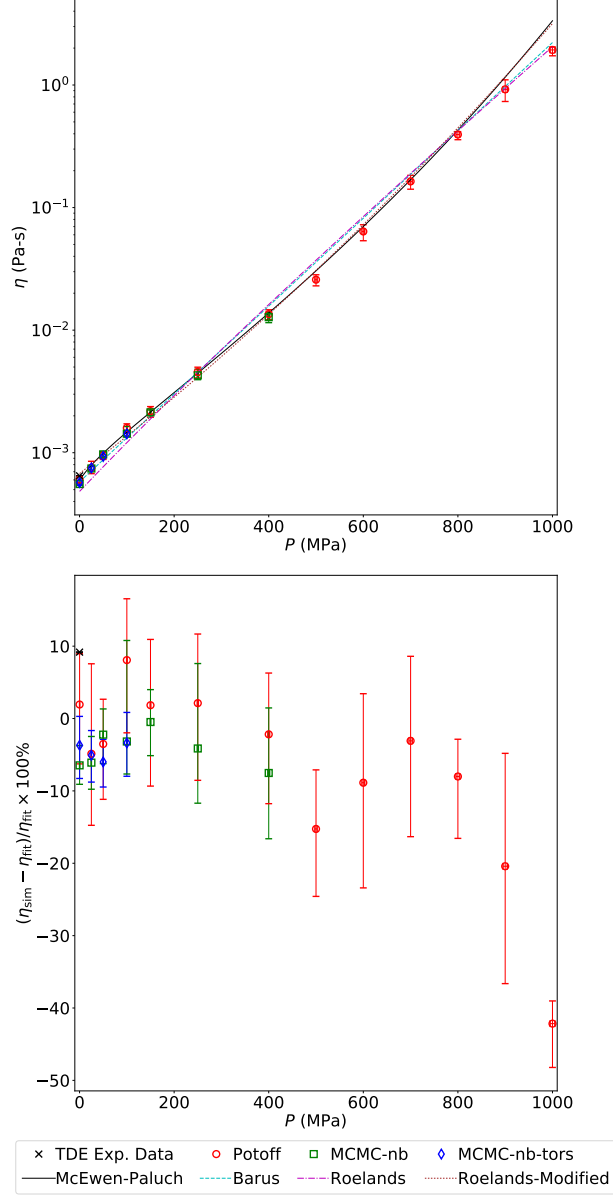
Figure 3: Viscosity-pressure results for Potoff, MCMC-Mie, and MCMC-Mie-tors. Different line colors and styles represent the best fit of Equations 9, 10, and 11.

Figure 4: Uncertainty distributions for Potoff, MCMC-Mie, and MCMC-Mie-tors.

the data are included in the training set while 30 % are excluded as the testing set. Since the mean-squared-error (MSE) for the training set is approximately equal to the MSE for the testing set, we conclude that the McEwen-Paluch model is not over-fit to the data.
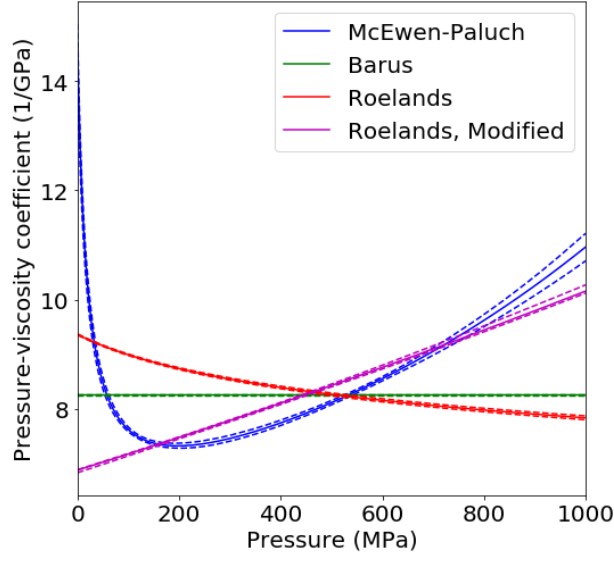
Figure 5: Pressure-viscosity coefficient predicted with Equations 9, 10, and 11.

Therefore, there is statistical evidence that the Mie 16-6 united-atom force field predicts an inflection point followed by super-Arrhenius behavior.
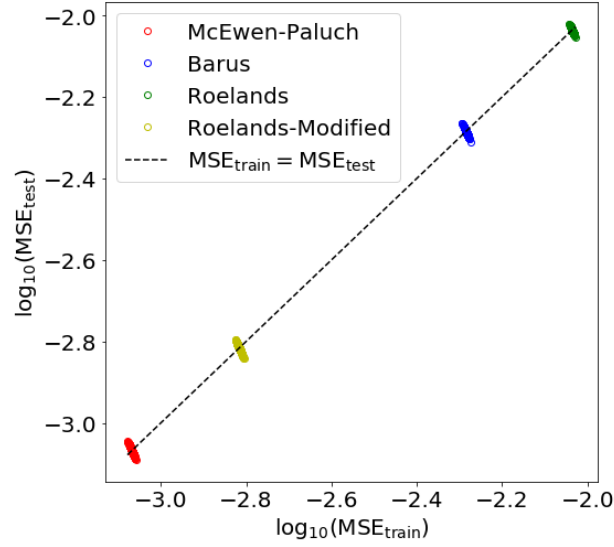

Figure 6: Monte Carlo cross-validation for Equations 9, 10, and 11.

4. Discussion

Although the Potoff force field demonstrates super-Arrhenius behavior, we should caution that this could be an anomaly of the force field. Since the Mie 16-6 potential is known to be overly repulsive at short distances, it is possible that this causes the sudden increase in viscosity. This has proven to be the case for the viscosity-density trend, although we have assumed that the viscosity-pressure trend is reliable due to the simultaneous over prediction of both viscosity and pressure at high densities.

Other studies [2] have corrected for systematic errors in viscosity by normalizing the viscosity-pressure trend with respect to viscosity at the lowest pressure. This approach would be possible for the challenge compound since a single experimental data point is available at saturation pressure. Although this may result in a more accurate prediction, we prefer to test the reliability of the Potoff force field without any empirical corrections since this serves to truly test its transferability and predictive capabilities.

The slow system dynamics at high pressures required extremely long simulations and large amounts of replicates. An attractive alternative is the so-called time-temperature superposition method, where simulations are performed at higher temperatures (to enhance the configurational sampling) and the viscosity at 293 K is obtained through extrapolation. Despite some obvious benefits, we are weary of the inordinately large uncertainties that this method can produce (see Figure 11 of Ref. 2). If there is any hope to determine the existence of super-Arrhenius behavior, the uncertainties at high pressures must be manageable. For this reason, we chose the more arduous brute-force approach.

5. Conclusions

Previous work demonstrated that the Potoff force field provides reliable viscosities (typically within 10 %) for well-studied n-alkane and branched alkanes both at saturation and elevated pressures. For this reason, the Potoff force field was chosen to predict the viscosity-pressure relationship of 2,2,4-trimethylhexane as part of the 10th Industrial Fluid Properties Simulation Challenge. In addition, we investigate the parameter uncertainty in

the simulation results with Bayesian inference. Specifically, the non-bonded and torsional potentials are varied from run to run according to a Markov Chain in force field parameter space.

Furthermore, we assess the existence of so-called super-Arrhenius behavior at high pressures. Cross validation model selection is employed to determine whether a super-Arrhenius empirical equation is required to reproduce our simulation results.

Supporting Information

Section SI.I provides GROMACS input files. Section SI.II outlines the Green-Kubo analysis process.

Acknowledgments

References

[1] Clare McCabe, Shengting Cui, Peter T. Cummings, Peter A. Gordon, and Roland B. Saeger. Examining the rheology of 9-octylheptadecane to giga-pascal pressures. *The Journal of Chemical Physics*, 114(4):1887–1891, 2001.

[2] Pinzhi Liu, Hualong Yu, Ning Ren, Frances E. Lockwood, and Q. Jane Wang. Pressure-viscosity coefficient of hydrocarbon base oil through molecular dynamics simulations. *Tribology Letters*, 60(3):34, 2015.

[3] M. G. Martin and J. I. Siepmann. Transferable potentials for phase equilibria. 1. United-atom description of *n*-alkanes. *The Journal of Physical Chemistry B*, 102(14):2569–2577, 1998.

[4] Marcus G. Martin and J. Ilja Siepmann. Novel configurational-bias monte carlo method for branched molecules. Transferable Potentials for Phase Equilibria. 2. United-Atom Description of Branched Alkanes. *The Journal of Physical Chemistry B*, 103(21):4508–4517, 1999.

[5] Mansi S. Shah, J. Ilja Siepmann, and Michael Tsapatsis. Transferable potentials for phase equilibria. Improved united-atom description of ethane and ethylene. *AIChE Journal*, 63(11):5098–5110, 2017.

[6] Andrea Hemmen and Joachim Gross. Transferable anisotropic united-atom force field based on the Mie potential for phase equilibrium calculations: *n*-alkanes and *n*-olefins. *The Journal of Physical Chemistry B*, 119(35):11695–11707, 2015.

[7] Dominik Weidler and Joachim Gross. Transferable anisotropic united-atom force field based on the Mie potential for phase equilibria: Aldehydes, ketones, and small cyclic alkanes. *Industrial & Engineering Chemistry Research*, 55(46):12123–12132, 2016.

[8] J. J. Potoff and D. A. Bernard-Brunel. Mie potentials for phase equilibria calculations: Applications to alkanes and perfluoroalkanes. *The Journal of Physical Chemistry B*, 113(44):14725–14731, 2009.

[9] Jason R. Mick, Mohammad Soroush Barhaghi, Brock Jackman, Loren Schwiebert, and Jeffrey J. Potoff. Optimized Mie potentials for phase equilibria: Application to branched alkanes. *Journal of Chemical & Engineering Data*, 62(6):1806–1818, 2017.

[10] Philippe Ungerer, Christele Beauvais, Jerome Delhommelle, Anne Boutin, Bernard Rousseau, and Alain H. Fuchs. Optimization of the anisotropic united atoms intermolecular potential for *n*-alkanes. *The Journal of Chemical Physics*, 112(12):5499–5510, 2000.

[11] Carlos Nieto-Draghi, Anthony Bocahut, Benoît Creton, Pascal Have, Aziz Ghoufi, Aurélie Wender, , Anne Boutin, Bernard Rousseau, and Laurent Normand. Optimisation of the dynamical behaviour of the anisotropic united atom model of branched alkanes: application to the molecular simulation of fuel gasoline. *Molecular Simulation*, 34(2):211–230, 2008.

[12] Richard A. Messerly, Michael R. Shirts, and Andrei F. Kazakov. Uncertainty quantification confirms unreliable extrapolation toward high pressures for united-atom Mie λ-6 force field. *Journal of Chemical Physics*, Pending publication, 2018.

[13] Peter A. Gordon. Development of intermolecular potentials for predicting transport properties of hydrocarbons. *The Journal of Chemical Physics*, 125(1):014504, 2006.

[14] Richard A. Messerly, Michelle C. Anderson, Mostafa S. Razavi, and J. Richard Elliott. Improvements and limitations of mie λ-6 potential for prediction of saturated and compressed liquid viscosity. *Fluid Phase Equilibria*, Pending publication, 2018.

[15] Carlos Nieto-Draghi, Philippe Ungerer, and Bernard Rousseau. Optimization of the anisotropic united atoms intermolecular potential for *n*-alkanes: Improvement of transport properties. *The Journal of Chemical Physics*, 125(4):044517, 2006.

[16] Carlos Braga and Karl P. Travis. Computer simulation of the role of torsional flexibility on mass and momentum transport for a series of linear alkanes. *The Journal of Chemical Physics*, 137(6):064116, 2012.

[17] Carmelo Herdes, Tim S. Totton, and Erich A. Müller. Coarse grained force field for the molecular simulation of natural gases and condensates. *Fluid Phase Equilibria*, 406:91 – 100, 2015.

[18] M. P. Allen and D. J. Tildesley. *Computer Simulation of Liquids*. Clarendon Press ; Oxford University Press, Oxford England New York, 1987.

[19] Richard A. Messerly, Thomas A. Knotts IV, and W. Vincent Wilding. Uncertainty quantification and propagation of errors of the Lennard-Jones 12-6 parameters for *n*-alkanes. *The Journal of Chemical Physics*, 146(19):194110, 2017.

[20] M.J. Abraham, D. van der Spoel, E. Lindahl, B.Hess, and the GROMACS development team. *GROMACS User Manual version 2018, www.gromacs.org (2018)*.

[21] GROMACS non-bonded tail corrections assume that the long-range contribution from the $r^{-\lambda}$ term is negligible compared to the r^{-6} term. By comparing the GROMACS output with other (slower) simulation packages, we verified that the small error introduced with this approximation does not significantly affect our results. For this reason, although it is straightforward to include the $r^{-\lambda}$ contribution, we did not attempt to modify the GROMACS default tail correction values.

[22] Berk Hess, Henk Bekker, Herman J. C. Berendsen, and Johannes G. E. M. Fraaije. LINCS: A linear constraint solver for molecular simulations. *Journal of Computational Chemistry*, 18(12):1463–1472, 1998.

[23] Berk Hess. P-LINCS: A parallel linear constraint solver for molecular simulation. *Journal of Chemical Theory and Computation*, 4(1):116–122, 2008.

[24] Edward J. Maginn, Richard A. Messerly, Daniel J. Carlson, Daniel R. Roe, and J. Richard Elliott. Best practices for computing transport properties 1. Self-diffusivity and viscosity from equilibrium molecular dynamics v1. *Living Journal of Computational Molecular Science*, Pending publication, 2018.

[25] Yong Zhang, Akihito Otani, and Edward J. Maginn. Reliable viscosity calculation from equilibrium molecular dynamics simulations: A time decomposition method. *Journal of Chemical Theory and Computation*, 11(8):3537–3546, 2015.

[26] C. Barus. Isothermals, isopiestics and isometrics relative to viscosity. *American Journal of Science*, 45:87–96, 1893.

[27] C.J.A. Roelands. *Correlational Aspects of the Viscosity-temperature-pressure Relationships of Lubricating Oils*. PhD thesis, TU Delft, Delft University of Technology, 1966.

[28] Scott Bair, Laetitia Martinie, and Philippe Vergne. Classical ehl versus quantitative ehl: A perspective part II-super-arrhenius piezoviscosity, an essential component of elastohydrodynamic friction missing from classical ehl. *Tribology Letters*, 63(3):37, 2016.